Noninvasive Autopsy-Validated Tumor Probability Maps Identify Glioma Invasion Beyond Contrast Enhancement

Samuel A. Bobholz, PhD [ORCID]*, Allison K. Lowman, BS*, Jennifer M. Connelly, MD‡, Savannah R. Duenweg, BS§, Aleksandra Winiarz, BS§, Biprojit Nath, MS§, Fitzgerald Kyereme, BS*, Michael Brehler, PhD*, John Bukowy, PhD||, Dylan Coss, MD¶, Janine M. Lupo, PhD#**, Joanna J. Phillips, MD, PhD‡‡§§, Benjamin M. Ellingson, PhD||||, Max O. Krucoff, MD¶¶, Wade M. Mueller, MD¶¶, Anjishnu Banerjee, PhD##, Peter S. LaViolette, PhD*§***

*Department of Radiology, Medical College of Wisconsin, Milwaukee, Wisconsin, USA; ‡Department of Neurology, Medical College of Wisconsin, Milwaukee, Wisconsin, USA; §Department of Biophysics, Medical College of Wisconsin, Milwaukee, Wisconsin, USA; ||Department of Electrical Engineering and Computer Science, Milwaukee School of Engineering, Milwaukee, Wisconsin, USA; ¶Department of Pathology, Medical College of Wisconsin, Milwaukee, Wisconsin, USA; #Department of Radiology and Biomedical Imaging, University of California, San Francisco, California, USA; **UCSF/UC Berkeley Graduate Program in Bioengineering, University of California, San Francisco and Berkeley, California, USA; ‡‡Department of Neurological Surgery, University of California, San Francisco, California, USA; §§Department of Pathology, University of California, San Francisco, California, USA; ||||UCLA Brain Tumor Imaging Laboratory, Department of Radiological Sciences, David Geffen School of Medicine, University of California Los Angeles, Los Angeles, California, USA; ¶¶Department of Neurosurgery, Medical College of Wisconsin, Milwaukee, Wisconsin, USA; ##Department of Biostatistics, Medical College of Wisconsin, Milwaukee, Wisconsin, USA; ***Department of Biomedical Engineering, Medical College of Wisconsin, Milwaukee, Wisconsin, USA

Correspondence: Peter S. LaViolette, PhD, Robert C. Olson MD Endowed Professor of Radiology, Medical College of Wisconsin, 8701 Watertown Plank Rd., Milwaukee, WI 53226, USA. Mail: plaviole@mcw.edu

BACKGROUND AND OBJECTIVES: This study identified a clinically significant subset of patients with glioma with tumor outside of contrast enhancement present at autopsy and subsequently developed a method for detecting nonenhancing tumor using radio-pathomic mapping. We tested the hypothesis that autopsy-based radio-pathomic tumor probability maps would be able to noninvasively identify areas of infiltrative tumor beyond traditional imaging signatures.

METHODS: A total of 159 tissue samples from 65 subjects were aligned to MRI acquired nearest to death for this retrospective study. Demographic and survival characteristics for patients with and without tumor beyond the contrast-enhancing margin were computed. An ensemble algorithm was used to predict pixelwise tumor presence from pathological annotations using segmented cellularity (Cell), extracellular fluid, and cytoplasm density as input (6 train/3 test subjects). A second level of ensemble algorithms was used to predict voxelwise Cell, extracellular fluid, and cytoplasm on the full data set (43 train/22 test subjects) using 5-by-5 voxel tiles from T1, T1 + C, fluid-attenuated inversion recovery, and apparent diffusion coefficient as input. The models were then combined to generate noninvasive whole brain maps of tumor probability.

RESULTS: Tumor outside of contrast was identified in 41.5% of patients, who showed worse survival outcomes (hazard ratio = 3.90, $P < .001$). Tumor probability maps reliably tracked nonenhancing tumor on a range of local and external unseen data, identifying tumor outside of contrast in 69% of presurgical cases that also showed reduced survival outcomes (hazard ratio = 1.67, $P = .027$).

CONCLUSION: This study developed a multistage model for mapping gliomas using autopsy tissue samples as ground truth, which was able to identify regions of tumor beyond traditional imaging signatures.

KEY WORDS: Artificial intelligence, Autopsy, Glioma, MRI, Pathology, Radiology

Glial brain tumors are the most common primary central nervous system tumors, with an incidence of around 6 per 100 000 persons.[1] High-grade gliomas such as glioblastomas (GBMs) are difficult to treat because of their aggressiveness and pathological heterogeneity, contributing to 1- and 5-year survival rates of 41% and 5%, respectively.[2,3] Current standard of care requires precise tumor localization to maximize efficacy of frontline treatments such as surgical resection and targeted radiation therapy. Studies examining resection extent in gliomas have demonstrated that maximizing tumor removal improves patient survival outcomes, underscoring the importance of identifying the full extent of gliomas.[4-7]

MRI is the primary method for noninvasively monitoring gliomas. Gadolinium contrast agents are used to highlight angiogenic disruptions in the blood-brain barrier, which results in an enhanced T1-weighted signal that defines the primary tumor mass.[8-10] Hyperintensities on T2-weighted fluid-attenuated inversion recovery (FLAIR) images correspond to a mixture of tumor and edema although differentiation remains difficult.[11-14] Apparent diffusion coefficient (ADC) images derived from diffusion-weighted imaging identify areas of diffusion restriction associated with hypercellularity although studies validating this beyond contrast-enhancing margins have suggested a weaker relationship.[14-18] Machine learning approaches have also sought to maximize the amount of clinically relevant information extracted from noninvasive imaging, using recent advances in computing to segment radiologist-defined margins, identify patient-level genetic signatures, and predict cellular-level information using biopsies as validation.[19-23]

Despite the promise of these recent techniques, identifying areas of tumor beyond contrast- and FLAIR-hyperintense margins remains difficult. Studies of autopsy samples aligned to MRI acquired near death found areas of active tumor as far as 10 cm beyond the treated margin, indicating need for tumor tracking improvements.[16,24,25] Therefore, studies with access to tissue beyond contrast enhancement are essential for identifying the true extent of tumor, particularly in the posttreatment state. This study uses autopsy tissue samples, collected within and beyond the traditional tumor margin, to assess the prevalence of tumor outside the MRI-defined margin and develop a multistage model for noninvasive tumor probability mapping. Specifically, we tested the hypothesis that an MRI-based model for tumor probability trained on autopsy tissue samples can track glioma invasion beyond the currently defined margin associated with worse prognoses.

METHODS

Patient Populations

This study was approved by the Institutional Review Board of the Medical College of Wisconsin. Written informed consent was obtained from 65 patients to participate in this study as part of our ongoing brain tumor bank starting in 2010, each diagnosed with a primary brain tumor. The study size was selected based on maximizing the number of complete imaging data sets with high-quality aligned tissue samples from autopsy. Clinical and demographic characteristics of this data set are presented in Table. Portions of this study sample have been used to explore radiopathomic characteristics in previous publications,[14,24] but this is the first study to develop noninvasive maps of tumor pathology using these data. Tumor probability map (TPM) software, study data, and other code required for preprocessing data will be made available on request.

MR Imaging Acquisition and Preprocessing

Clinical imaging was collected from each patient's last MRI session before death. T1, T1 + C, FLAIR, and ADC images were selected as input for this study because they provide a wide range of information regarding tissue characteristics while remaining ubiquitous across clinical acquisitions. T1, T1 + C, and ADC images were each rigidly aligned to the FLAIR image using SPM12 (https://www.fil.ion.ucl.ac.uk/spm/software/spm12/). Qualitative images (T1, T1 + C, and FLAIR) were then divided by the intensity SD within the brain to normalize values across patients.[8,14]

Tissue Segmentation and Processing

A total of 159 tissue samples were collected at autopsy using previously published methods.[14,16,25] Board-certified pathologists (EJC, DC) collected large-format tissue samples, with additional MRI-based sampling guidance from research staff (PSL, AKL, SAB). Tissue samples were processed, digitized, and segmented using a previously published tool.[24] Additionally, 33 tissue samples from a subset of 9 participants were annotated for the presence of infiltrative tumor, tumor with pseudopalisading necrosis (PN), nontumor necrosis, and unlabeled tissue by a pathologist-trained technician (AKL).

MRI Histology Coregistration

Tissue samples were aligned to each participant's FLAIR image using previously published MATLAB (MathWorks Inc.) software.[14,16,25-27] Manually defined control points were used to identify architectural landmarks on the tissue data and MRI using autopsy images to guide accurate placement. Control points were used to compute a nonlinear

TABLE. Demographic and Clinical Information for the Study Sample		
	Train	**Test**
Number of patients	43	22
Age (y)	58.4 (14.1)	60.9 (11.7)
Overall survival (mo)	48.8 (71.2)	34.8 (42.3)
Time between MRI and death (d)	78.8 (73.6)	69.6 (66.5)
GBM/non-GBM	29/14	18/4
Radiation (yes/no)	39/4	21/1
Chemotherapy (yes/no)	39/4	20/2
Bevacizumab (yes/no)	34/9	15/7
Tumor treating fields (yes/no)	17/26	6/16

GBM, glioblastoma.

transform that warped tissue to the same space as the MRI, and regions of interest were drawn to exclude areas of tissue distortion (ie, rips, folds) and MRI artifacts. After MRI-tissue coregistration, all MRI and tissue data were resampled to 0.4397 × 0.4397 mm per pixel resolution to harmonize all subjects to the most common acquisition parameters.

Assessing Prevalence of Tumor Beyond MRI-Defined Margin

Aligned autopsy tissue was compared with the T1 + C MRI to estimate the prevalence of tumor outside of contrast enhancement (TOC). Tissue samples were inspected for tumor presence using histological characteristics and available immunohistochemical staining (ie, Ki-67, CD31). Patients were coded for the presence of TOC by comparing manually segmented maps of contrast with aligned tissue samples. χ^2 tests were used to determine differences in TOC frequency among patients who did and did not receive radiation with temozolomide (Rad + temozolomide [TMZ]), bevacizumab (Bev), and tumor treating fields (TTFields), as well as among diagnostic grade groups. A Cox proportional hazards regression was fit to compare survival durations between patients with and without TOC, including time between MRI and death as a covariate. Survival curves were limited to patients who received standard treatment (Rad + TMZ) to exclude a small number of untreated patients who survived shorter than similarly treated patients. Analysis was performed for the full data set (N = 65), as well as on subjects with scans less than 90 days before death (N = 47) and patients with a primary GBM at first surgery (N = 37) to compare results across potential confounds.

Predicting Tumor Presence from Pathological Segmentations

A chart indicating the flow of patients across the multiple model training stages is presented in **Supplemental Digital Content 1** (http://links.lww.com/NEU/E159). The first component of the multistage tumor prediction model involved predicting tumor annotations from the segmented pathology data. Several different candidate models were assessed, including k-nearest neighbors, naïve bayes, decision trees, and random-under-sampling-boosted random forest (random undersampled [RUS] Tree) models. Each model was trained using pixelwise cellularity, cytoplasm (Cyt) density, and extracellular fluid (ECF) density as input to predict tumor (infiltrative tumor/PN) vs nontumor (nontumor necrosis/unlabeled). Models were trained on slides from 6 subjects and validated on the 3 remaining subjects. Model performance was evaluated using receiver operator characteristic plots and area under the curve (AUC) metrics. The model with the highest AUC was then incorporated into the multistage model.

Predicting Pathological Segmentations from MRI Data

The second stage of the multistage model focused on training separate models to predict cell, Cyt, and ECF density using MRI data. Bootstrap aggregating random forest models were trained to predict voxelwise densities using 5-by-5 voxel tiles from T1, T1 + C, FLAIR, and ADC as input. This framework was selected based on our previous publication, which developed a proof of concept for predicting cellularity using MRI data in a smaller patient sample.[24] These models were developed on 2/3rd of the full data set (n = 43) and tested on the heldout set (n = 22) to assess generalizability. No patients in the pathological tumor prediction test set overlapped with the training set for these radio-pathomic models, ensuring that the test set contained only data unseen in training for every

component model. Quantitative performance was evaluated using root mean squared error (RMSE) estimates within each test set subject, and example segmentations were plotted and compared with ground truth segmentations.

Predicting Tumor Presence from MRI Data

After model training, the best performing pathological tumor prediction model was used to convert whole brain cell, ECF, and Cyt density maps to TPMs. These maps were plotted against ground truth tissue segmentations and annotations to assess accuracy at identifying novel tumor areas. In addition, TPMs were generated for 3 external subjects to assess the quality of the maps and ability to identify nonenhancing tumor on MRI data acquired at other institutions. The first external subject was a 61-year-old male diagnosed with a recurrent GBM, whose scan was collected by our external collaborators at the University of California, Los Angeles. The second external case was a pretreatment acquisition from a 50-year-old male diagnosed with GBM, taken from the publicly available TCGA-GBM data set (https://cancergenome.nih.gov/).[28,29] The third case was a 53-year-old female diagnosed with an IDH1 wild-type GBM, whose scan was collected by an external collaborator from University of California, San Francisco, for which biopsy data from surgical resection were available for an area beyond contrast enhancement. Finally, TPMs were generated from an independent local data set of 84 GBM cases[30] with imaging acquired presurgery to determine areas of predicted tumor outside of contrast enhancement (pTOC). A Kaplan–Meier curve was fit to assess differences in overall survival between patients with and without pTOC (n = 58 and 26, respectively).
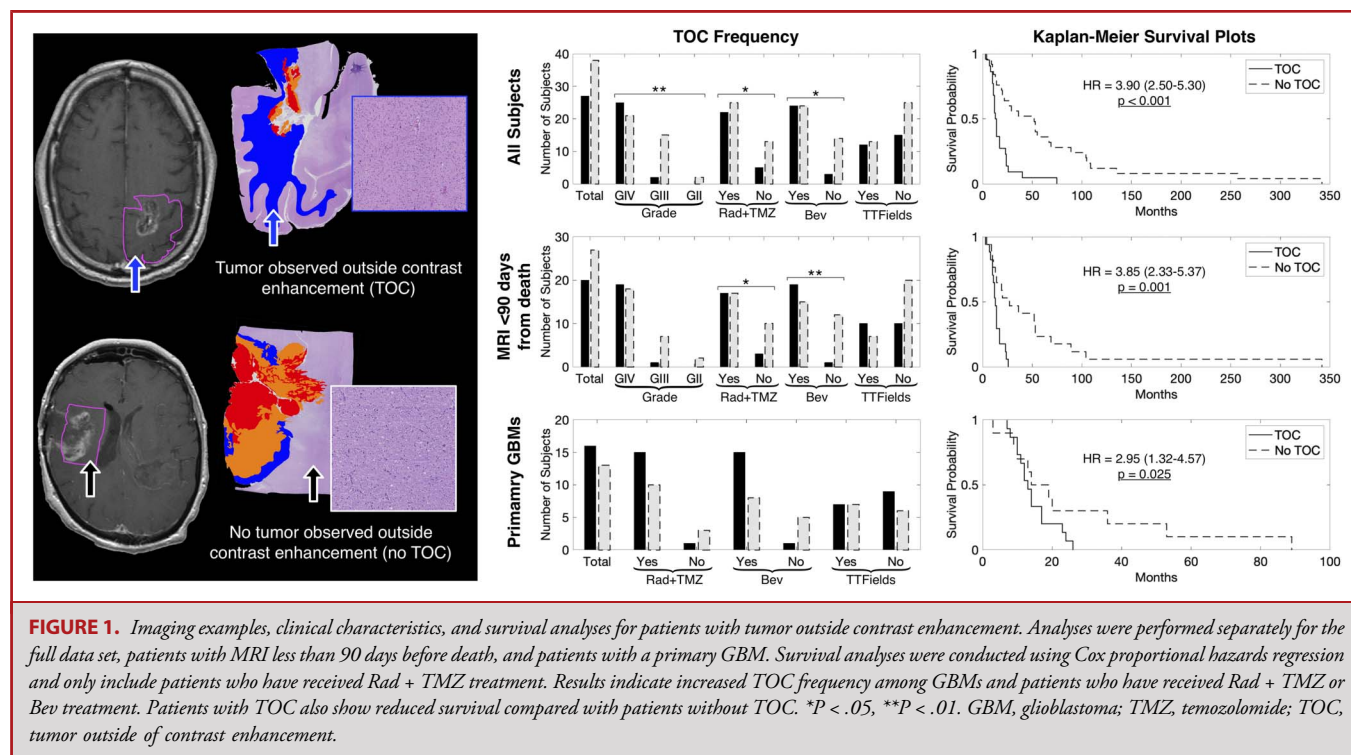
RESULTS

Prevalence of Nonenhancing Tumor

Figure 1 shows prevalence estimates for TOC presence and corresponding Kaplan–Meier plots for survival analyses. TOC was observed in 41.5% of patients, with increased presence among patients with GBM (G4) (χ^2 = 10.73, P = .005), patients treated with Rad + TMZ (χ^2 = 3.99, P = .046), and patients treated with bevacizumab (Bev) (χ^2 = 5.41, P = .020). Treated patients with TOC showed decreased survival rates compared with patients without TOC (hazard ratio = 3.90, 95% CI = 2.50-5.30, P < .001). Patients with MRI data within 90 days of death also showed increased TOC presence among Rad-TMZ and bevacizumab-treated (χ^2 = 4.50, P = .033 and χ^2 = 4.50, P = .033, respectively) patients and reduced survival associated with TOC (hazard ratio = 3.85, 95% CI = 2.33-5.37, P = .001). Patients with primary GBM did not show significant differences in TOC presence for treatment but showed reduced survival within patients with TOC (hazard ratio = 2.95, 95% CI = 1.32-4.57, P = .025).

Predicting Tumor Presence from Pathological Segmentations

Figure 2 shows performance results for the pathological tumor prediction model, along with example TPMs and ground truth annotations. The RUS Tree model gave the best receiver operator characteristic AUC of 0.857 and was therefore selected as the

FIGURE 1. *Imaging examples, clinical characteristics, and survival analyses for patients with tumor outside contrast enhancement. Analyses were performed separately for the full data set, patients with MRI less than 90 days before death, and patients with a primary GBM. Survival analyses were conducted using Cox proportional hazards regression and only include patients who have received Rad + TMZ treatment. Results indicate increased TOC frequency among GBMs and patients who have received Rad + TMZ or Bev treatment. Patients with TOC also show reduced survival compared with patients without TOC. *P < .05, **P < .01. GBM, glioblastoma; TMZ, temozolomide; TOC, tumor outside of contrast enhancement.*

model used to convert MRI-based pathological segmentations into TPMs. Example predictions show good concordance between areas of high tumor probability and actual tumor presence within both infiltrative tumor and PN, while correctly avoiding edema and other nontumor areas.

Predicting Pathological Segmentations from MRI Data

Segmentation prediction results are shown in Figure 3, along with example whole brain predictions on test set subjects. Each radio-pathomic model had a mean subject-level RMSE value within a SD of the ground truth (cell RMSE = 0.756; Cyt RMSE = 0.917; ECF RMSE = 0.941), indicating satisfactory model performance for each tissue type. Example predictions indicate regions where these maps improve pathological interpretations of the MRI data, such as discrimination between areas of edema and hypercellularity within the FLAIR hyperintense region and hypercellularity beyond contrast enhancement.

Predicting Tumor Presence from MRI Data

An example TPM generated from the full multistage model is presented in Figure 4. Test set TPM with pathological annotations available showed good correspondence between areas of predicted and actual tumors, with separation between areas of PN (high cellularity, high ECF) and areas of non-PN tumor (high cellularity, normal ECF) seen on the corresponding segmentation maps. Tumor was also accurately observed in an area without contrast enhancement. TPMs for patients with imaging acquisitions close to

death are presented in Figure 5. The first example shows a case of successfully identified tumor outside contrast that extends beyond the FLAIR hyperintense region. The second example demonstrates the ability for TPMs to both identify tumor within enhancement and avoid false positives, as well as identify edges of the tumor with increased proliferation relative to others. The third example shows a false positive from the model, where the model labels a region containing a mixture of nonenhancing tumor and reactive gliosis that is entirely labeled as tumor, indicating a potential source of error in the model. Additional TPMs for external data and survival analysis for pTOC are presented in Figure 6. Predictions on external data sets demonstrated that TPMs generated from this framework provided low-noise, interpretable maps on new data and identified new areas of possible tumor infiltration in an area without contrast enhancement. Biopsy data from an area of predicted high tumor probability on the UCSF subject was pathologically confirmed as tumor, with a Ki-67 positive staining rate of 13%. Survival analyses for presurgical cases revealed that patients with pTOC demonstrated worse overall survival than patients without pTOC (hazard ratio = 1.67, CI = 1.07-2.62, P = .027).

DISCUSSION

Key Results

This study developed a multistage predictive model that identifies areas of tumor beyond traditional imaging signatures.
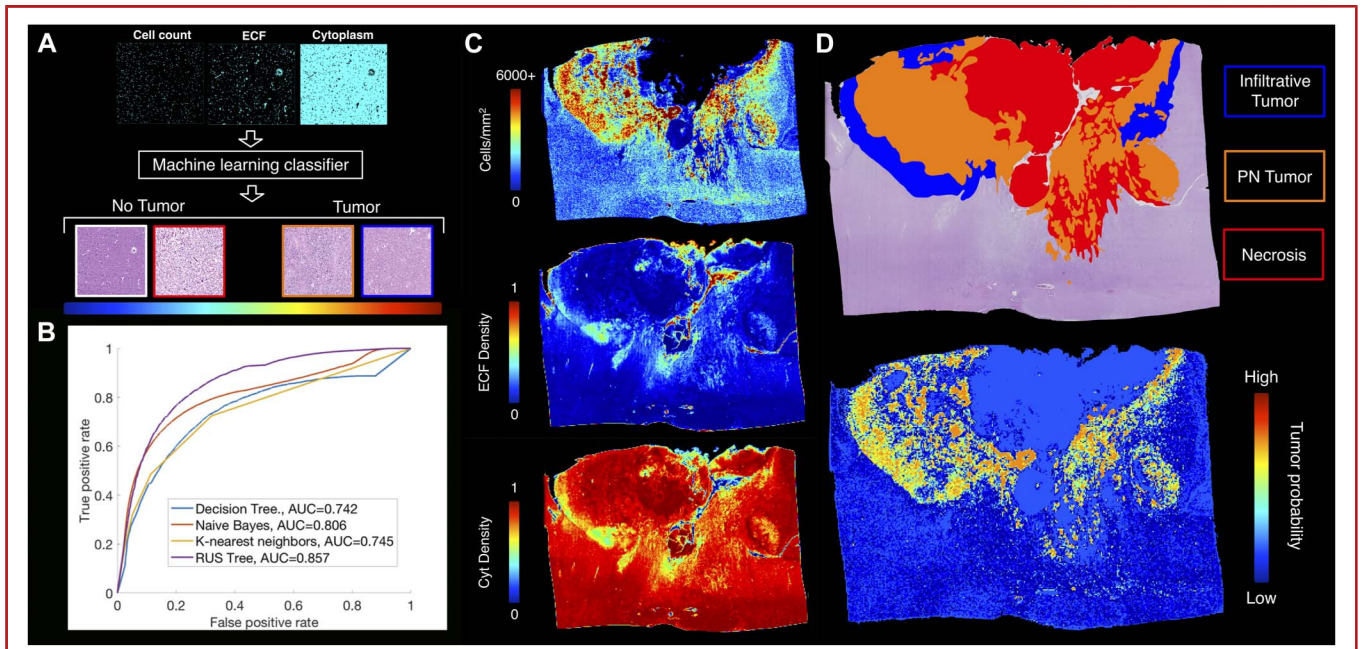
FIGURE 2. *Pathological tumor prediction.* **A,** *The pathological tumor prediction model uses cell density, ECF, and Cyt segmentations to distinguish tumor vs nontumor using the pathological annotations as ground truth.* **B,** *The RUS Tree algorithm was the highest-performing tumor prediction model (AUC = 0.857) and was used in the final multistage TPM model.* **C,** *Example segmentations and* **D,** *TPMs from the RUS Tree model show accurate tumor prediction in both infiltrative tumor and PN areas, while avoiding both normal tissue and areas of necrosis. AUC, area under the curve; Cyt, cytoplasm; ECF, extracellular fluid; PN, pseudopalisading necrosis; RUS, random undersampled; TPM, tumor probability map.*

A pathological tumor prediction model based on histology segmentations was combined with MRI-based maps of tissue composition to bridge the gap between histopathological assessment and noninvasive glioma tracking. We validated this technique using autopsy tissue samples as ground truth and successfully applied our models to external data to demonstrate generalizability. This study is the first of its kind to provide TPMs validated using tissue well beyond the current treatment margin, and is, to date, the largest study of radio-pathomic signatures at autopsy in brain cancer.

Interpretation

Autopsy-based TPMs have several benefits compared with other techniques for identifying tumor extent. Contrast-based methods such as traditional T1-weighted contrast enhancement and dynamic susceptibility-based perfusion imaging both rely on disruptions in the blood brain barrier to highlight regions of vascular tumor, which are prone to both missing areas of nonangiogenic infiltration and false positives (ie, pseudoprogression) after radiation and other treatments.[31-33] TPMs can apply the same set of weights across the brain based on data-driven texture features that identify areas of tumor in both the presence and absence of contrast enhancement, indicating novel radiographic signatures that function in the absence of angiogenic activity, which is particularly useful for nonenhancing low-grade glioma cases. While other studies have developed radio-pathomic approaches to identifying tumor presence, many of these tools have been developed on pretreatment biopsy tissue, which is prone to

misregistration errors and loss of orientation information, and typically offer only a single data point per pathological sample.[18,20,34-37] Furthermore, these samples are extracted from regions that are already surgically viable and therefore are yet to be validated on suspected normal tissue beyond the identifiable tumor margin. The use of autopsy tissue, while adding timing of tissue collection as an important source of uncertainty, allows for unprecedented tissue alignment, extent of sampling, and pathological richness because our data set includes over 2 million voxels with matched pathology. Several advanced imaging tools have also been proposed to probe new areas of tumor biology to circumvent the restrictions of contrast-based methods, including pH-based amide proton transfer chemical exchange saturation transfer[38,39] imaging and MR spectroscopy–based measures of tumor metabolism.[40-42] However, these tools often require substantial effort to implement to introduce the tools and protocols required for clinical translation and often increase both scan time and cost of acquisition. Because TPMs only require standard imaging contrasts to extract novel texture information, they can be applied on most clinical MRI sessions without additional scan time and can be applied to longitudinal and retrospective scans for rapid validation at many institutions.

Generalizability

This technology has several use cases in both clinical and research settings. The use of TPMs to identify the full extent of nonenhancing tumor regions can be used in surgical planning in
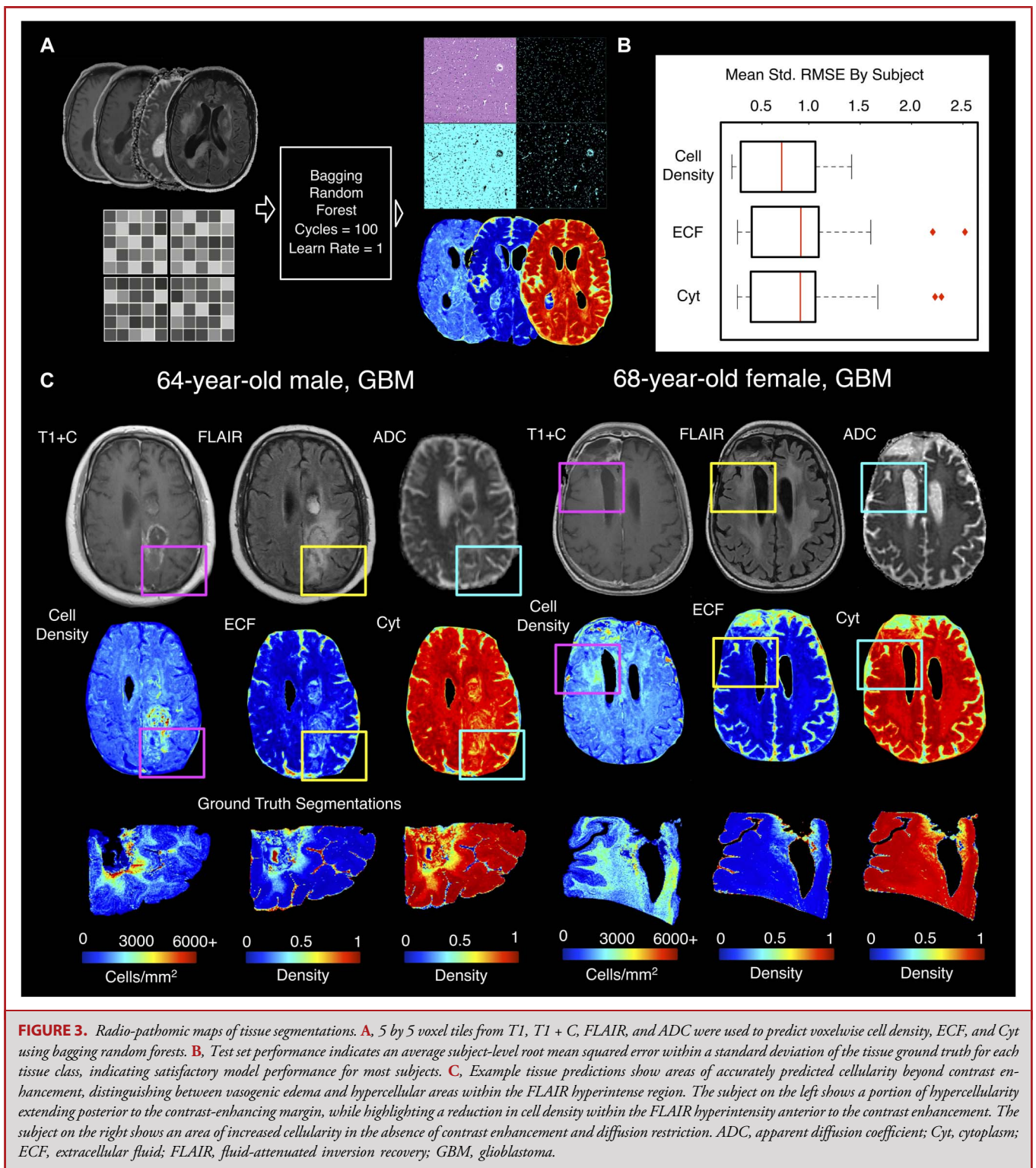
FIGURE 3. *Radio-pathomic maps of tissue segmentations. **A**, 5 by 5 voxel tiles from T1, T1 + C, FLAIR, and ADC were used to predict voxelwise cell density, ECF, and Cyt using bagging random forests. **B**, Test set performance indicates an average subject-level root mean squared error within a standard deviation of the tissue ground truth for each tissue class, indicating satisfactory model performance for most subjects. **C**, Example tissue predictions show areas of accurately predicted cellularity beyond contrast enhancement, distinguishing between vasogenic edema and hypercellular areas within the FLAIR hyperintense region. The subject on the left shows a portion of hypercellularity extending posterior to the contrast-enhancing margin, while highlighting a reduction in cell density within the FLAIR hyperintensity anterior to the contrast enhancement. The subject on the right shows an area of increased cellularity in the absence of contrast enhancement and diffusion restriction. ADC, apparent diffusion coefficient; Cyt, cytoplasm; ECF, extracellular fluid; FLAIR, fluid-attenuated inversion recovery; GBM, glioblastoma.*

conjunction with fluorescence-based guidance to help plan supramarginal resections because this would allow visualization of distant tumor areas where fluorescence would not be seen from the main resection cavity. In addition, this tool is useful postsurgery in the planning of radiation dosing because the current standard of high-dose administration to the contrast-enhancing
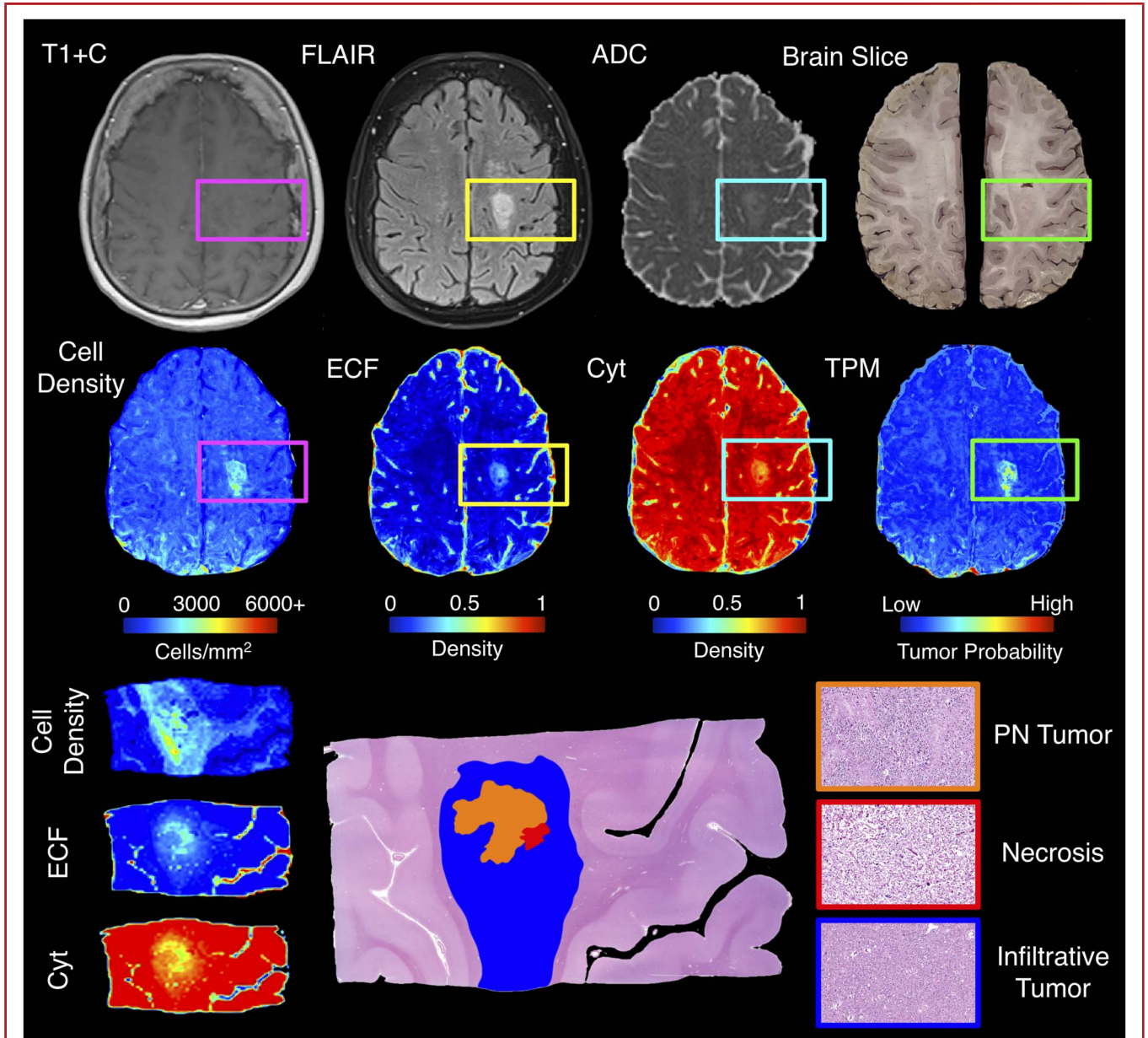
FIGURE 4. *Example TPM for a test set subject (GBM, Female, 80yo), along with corresponding MRI and segmentation predictions. The TPM for this patient accurately highlights an area of tumor outside contrast enhancement and in the absence of diffusion restriction. In addition, the cell density map highlights that the entire tumor area is hypercellular, whereas the ECF map highlights a high-ECF core to the hypercellular area, which correctly suggests an area of PN (high cellularity, high ECF). This demonstrates the ability for TPMs to distinguish between pathologically distinct regions of tumor. Cyt, cytoplasm; ECF, extracellular fluid; FLAIR, fluid-attenuated inversion recovery; PN, pseudopalisading necrosis; TPM, tumor probability map.*

region and low-dose administration to FLAIR hyperintensity runs the risk of both underdosing nonenhancing tumor and radiating normal tissue. Because TPMs can differentiate between tumor and nontumor components of the FLAIR-enhancing region, it may be able to spare eloquent tissue while providing the full radiation dose to occult tumor areas. Use cases in the research setting include further understanding the molecular, genetic, and demographic factors that impact the degree of nonenhancing tumor presence across tumor types, as well as better understanding on how nonenhancing tumor affects prognosis. Critically, this tool has the potential to visualize the impact of treatment on the full extent of tumor infiltration postradiation and
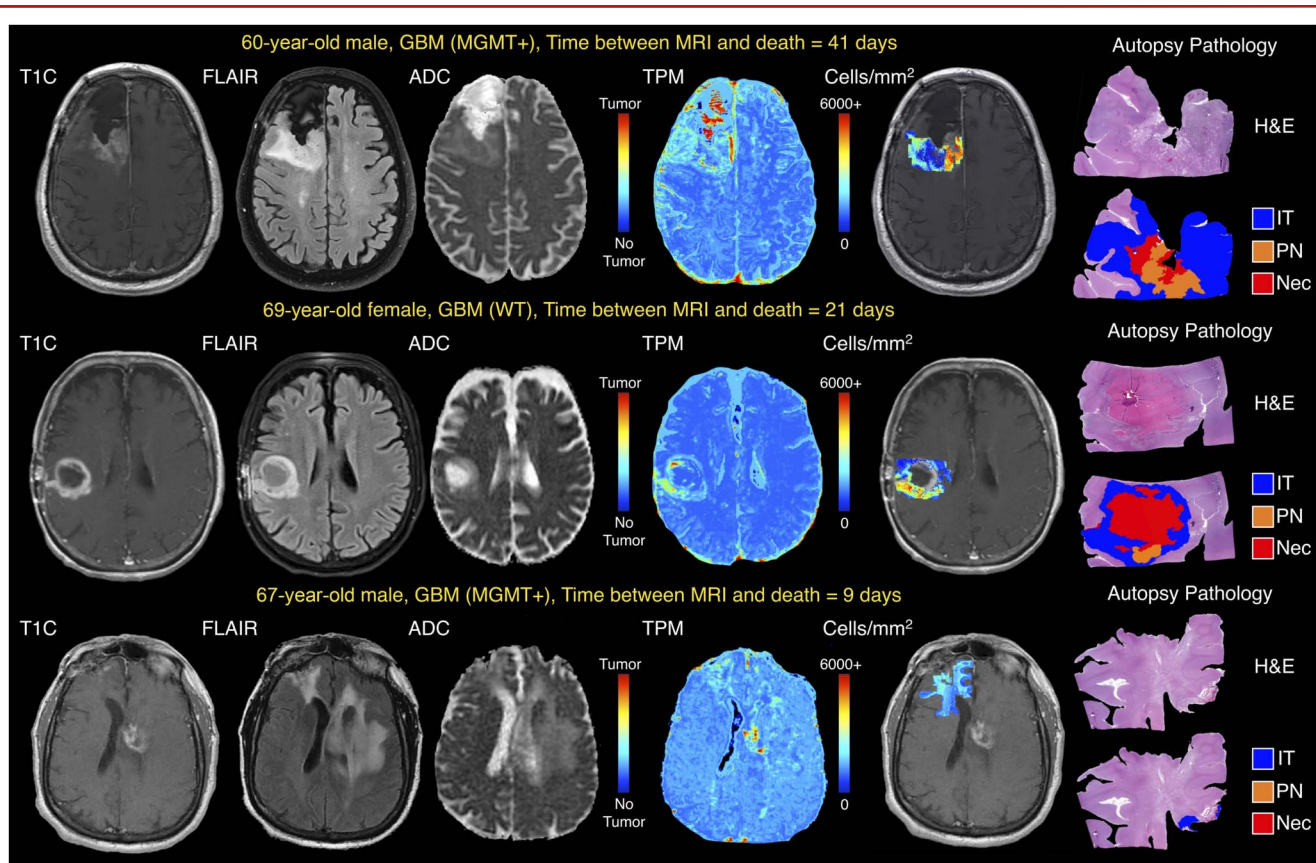
FIGURE 5. *Example TPMs for 3 individuals. The first case presents an area of high tumor probability outside of contrast enhancement, avoiding a central necrotic area and identifying tumor extent that goes beyond the FLAIR hyperintense signal with pathological conformation of tumor presence. The second case shows high tumor probability well circumscribed within the contrast-enhancing lesion, correctly identifying a lack of tumor outside of contrast in this area while highlighting increased cellularity in the posterior edge of the tumor relative to the anterior. The third case not only shows an area of high tumor probability in an area with some tumor invasion but also includes reactive gliosis in the high tumor probability area, indicating a representative false positive. FLAIR, fluid-attenuated inversion recovery; PN, pseudopalisading necrosis; TPM, tumor probability map.*

postantiangiogenic therapy, and future research developing treatment response metrics for later-stage interventions may improve detection of therapeutic benefit.

Limitations

Because of the use of autopsy tissue samples, the time between imaging and death is an important limiting factor in this study. We have accounted for this in our study by reproducing our frequency assessment of TOC and its impact on survival to imaging within 3 months of death and have matched our train and test data sets for time between MRI and death. Future studies using longitudinal imaging to model tumor growth rates that can then extend the imaging-defined margins to their full extent at death may control for this factor more precisely. Incorporating biopsy tissue from earlier clinical timepoints may also provide control over time between MR and death by including tissue and MRI data collected

simultaneously. Potential tissue distortions may result in imperfect alignment with MRI data; however, our previously published tissue processing protocol controls for this at every step of tissue collection, and regions of interest defined after warping are used to exclude regions of suboptimal tissue quality. Future research will also be essential for determining how well the model operates in both the presence and absence of angiogenic activity, as well as in conjunction with other treatments. In addition, while this study has found a link between nonenhancing tumor presence and overall survival, it is likely underpowered to account for a range of common factors such as Karnofsky Performance Status or genetic signatures such as isocitrate dehydrogenase 1 mutation status and O[6]-methylguanine-DNA methyltransferase methylation status. Applying these models to large, publicly available data sets will allow for large-scale validation of this signature's prognostic value in relation to these potentially confounding effects.
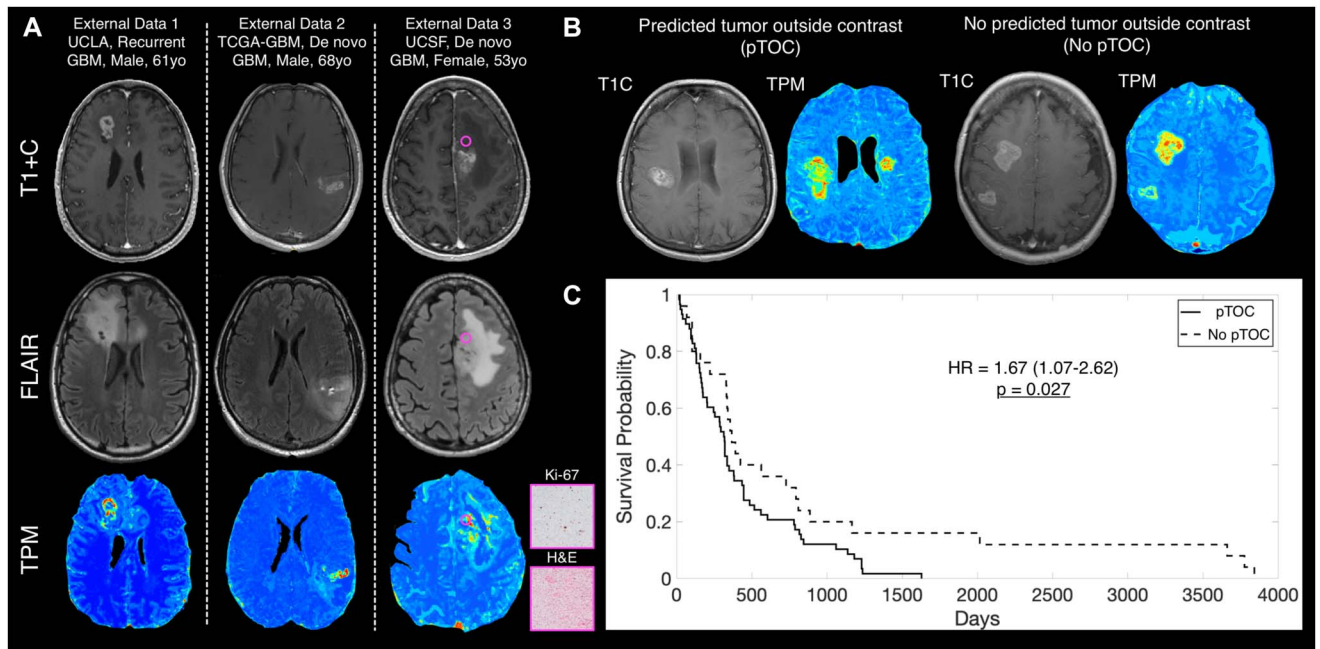
FIGURE 6. *External TPMs and survival analyses for predicted tumor outside of contrast enhancement presurgery.* **A**, *Example TPMs applied to externally collected data show similar-quality TPMs to those included in our study and show areas of predicted tumor beyond contrast enhancement. External Data 3 show additional histology from biopsy-confirmed tumor in a nonenhancing area of predicted high tumor probability presurgery.* **B**, *Examples of pTOC and no pTOC, showing patients with predicted nonenhancing tumor presence compared with patients with no predicted tumor presence outside of contrast enhancement.* **C**, *Kaplan–Meier survival curves showing longer overall survival in patients with pTOC presurgery (HR = 1.67 (1.07-2.62), P = .027), similar to the pattern observed with autopsy-confirmed tumor outside contrast before death seen in Figure 1. FLAIR, fluid-attenuated inversion recovery; GBM, glioblastoma; HR, hazard ratio; PN, pseudopalisading necrosis; pTOC, predicted tumor outside of contrast enhancement; TPM, tumor probability map.*

CONCLUSION

Autopsy tissue samples aligned to MRI were used to develop a multistage model for tumor probability to predict areas of non-enhancing tumor in patients with glioma. This technique has the potential to improve disease tracking and could expand the treated margin to encompass additional infiltrative tumor missed by current tracking techniques.

Funding

Disclosures

REFERENCES

1. Ostrom QT, Cioffi G, Gittleman H, et al. CBTRUS statistical report: primary brain and other central nervous system tumors diagnosed in the United States in 2012-2016. *Neuro Oncol.* 2019;21(Suppl 5):v1-v100.
2. Ostrom QT, Cote DJ, Ascha M, Kruchko C, Barnholtz-Sloan JS. Adult glioma incidence and survival by race or ethnicity in the United States from 2000 to 2014. *JAMA Oncol.* 2018;4(9):1254-1262.
3. Mathew EN, Berry BC, Yang HW, Carroll RS, Johnson MD. Delivering therapeutics to glioblastoma: overcoming biological constraints. *Int J Mol Sci.* 2022; 23(3):1711.
4. Behling F, Rang J, Dangel E, et al. Complete and incomplete resection for progressive glioblastoma prolongs post-progression survival. *Front Oncol.* 2022;12:755430.
5. Karschnia P, Vogelbaum MA, van den Bent M, et al. Evidence-based recommendations on categories for extent of resection in diffuse glioma. *Eur J Cancer.* 2021;149:23-33.
6. Aabedi AA, Young JS, Zhang Y, et al. Association of neurological impairment on the relative benefit of maximal extent of resection in chemoradiation-treated newly diagnosed isocitrate dehydrogenase wild-type glioblastoma. *Neurosurgery.* 2022; 90(1):124-130.
7. Skardelly M, Kaltenstadler M, Behling F, et al. A continuous correlation between residual tumor volume and survival recommends maximal safe resection in glioblastoma patients: a nomogram for clinical decision making and reference for non-randomized trials. *Front Oncol.* 2021;11:748691.
8. Ellingson BM, Aftab DT, Schwab GM, et al. Volumetric response quantified using T1 subtraction predicts long-term survival benefit from cabozantinib monotherapy in recurrent glioblastoma. *Neuro Oncol.* 2018;20(10):1411-1418.
9. Tixier F, Um H, Young RJ, Veeraraghavan H. Reliability of tumor segmentation in glioblastoma: impact on the robustness of MRI-radiomic features. *Med Phys.* 2019; 46(8):3582-3591.

10. He L, Huang Y, Ma Z, Liang C, Liang C, Liu Z. Effects of contrast-enhancement, reconstruction slice thickness and convolution kernel on the diagnostic performance of radiomics signature in solitary pulmonary nodule. *Sci Rep.* 2016;6:34921.

11. Husstedt HW, Sickert M, Köstler H, Haubitz B, Becker H. Diagnostic value of the fast-FLAIR sequence in MR imaging of intracranial tumors. *Eur Radiol.* 2000;10(5):745-752.

12. Garrett MD, Yanagihara TK, Yeh R, et al. Monitoring radiation treatment effects in glioblastoma: FLAIR volume as significant predictor of survival. *Tomography.* 2017;3(3):131-137.

13. Hawkins-Daarud A, Rockne RC, Anderson ARA, Swanson KR. Modeling tumor-associated edema in gliomas during anti-angiogenic therapy and its impact on imageable tumor. *Front Oncol.* 2013;3:66.

14. Bobholz SA, Lowman AK, Barrington A, et al. Radiomic features of multi-parametric MRI present stable associations with analogous histological features in patients with brain cancer. *Tomography.* 2020;6(2):160-169.

15. Galla N, Chiang G, Chakraborty S, et al. Apparent diffusion coefficient changes predict survival after intra-arterial bevacizumab treatment in recurrent glioblastoma. *Neuroradiology.* 2017;59(5):499-505.

16. LaViolette PS, Mickevicius NJ, Cochran EJ, et al. Precise ex vivo histological validation of heightened cellularity and diffusion-restricted necrosis in regions of dark apparent diffusion coefficient in 7 cases of high-grade glioma. *Neuro Oncol.* 2014;16(12):1599-1606.

17. Chenevert TL, Malyarenko DI, Galbán CJ, et al. Comparison of voxel-wise and histogram analyses of glioma ADC maps for prediction of early therapeutic change. *Tomography.* 2019;5(1):7-14.

18. Eidel O, Neumann JO, Burth S, et al. Automatic analysis of cellularity in glioblastoma and correlation with ADC using trajectory analysis and automatic nuclei counting. *PLoS One.* 2016;11(7):e0160250.

19. Bakas S, Reyes M, Battistella E, et al. Identifying the best machine learning algorithms for brain tumor segmentation, progression assessment, and overall survival prediction in the BRATS challenge. Vol abs/1811. 2018. http://arxiv.org/abs/1811.02629

20. Gates EDH, Lin JS, Weinberg JS, et al. Guiding the first biopsy in glioma patients using estimated Ki-67 maps derived from MRI: conventional versus advanced imaging. *Neuro Oncol.* 2019;21(4):527-536.

21. Booth TC, Grzeda M, Chelliah A, et al. Imaging biomarkers of glioblastoma treatment response: a systematic review and meta-analysis of recent machine learning studies. *Front Oncol.* 2022;12:799662.

22. Kickingereder P, Neuberger U, Bonekamp D, et al. Radiomic subtyping improves disease stratification beyond key molecular, clinical, and standard imaging characteristics in patients with glioblastoma. *Neuro Oncol.* 2018;20(6):848-857.

23. Rathore S, Akbari H, Rozycki M, et al. Radiomic MRI signature reveals three distinct subtypes of glioblastoma with different clinical and molecular characteristics, offering prognostic value beyond IDH1. *Sci Rep.* 2018;8(1):5087.

24. Bobholz SA, Lowman AK, Brehler M, et al. Radio-pathomic maps of cell density identify brain tumor invasion beyond traditional MRI-defined margins. *AJNR Am J Neuroradiol.* 2022;43(5):682-688.

25. Nguyen HS, Milbach N, Hurrell SL, et al. Progressing bevacizumab-induced diffusion restriction is associated with coagulative necrosis surrounded by viable tumor and decreased overall survival in patients with recurrent glioblastoma. *AJNR Am J Neuroradiol.* 2016;37(12):2201-2208.

26. McGarry SD, Bukowy JD, Iczkowski KA, et al. Radio-pathomic mapping model generated using annotations from five pathologists reliably distinguishes high-grade prostate cancer. *J Med Imaging.* 2020;7(5):054501-054511.

27. McGarry SD, Bukowy JD, Iczkowski KA, et al. Gleason probability maps: a radiomics tool for mapping prostate cancer likelihood in MRI space. *Tomography.* 2019;5(1):127-134.

28. Clark K, Vendt B, Smith K, et al. The cancer imaging archive (TCIA): maintaining and operating a public information repository. *J Digit Imaging.* 2013;26(6):1045-1057.

29. Scarpace L, Mikkelsen T, Cha S, et al. *Radiology Data from the Cancer Genome Atlas Glioblastoma Multiforme [TCGA-GBM] Collection.* 2016. https://wiki.cancerimagingarchive.net/x/sgAe

30. McGarry SD, Hurrell SL, Kaczmarowski AL, et al. Magnetic resonance imaging-based radiomic profiles predict patient prognosis in newly diagnosed glioblastoma before therapy. *Tomography.* 2016;2(3):223-228.

31. Blasel S, Zagorcic A, Jurcoane A, et al. Perfusion MRI in the evaluation of suspected glioblastoma recurrence. *J Neuroimaging.* 2016;26(1):116-123.

32. Zhang J, Liu H, Tong H, et al. *Clinical Applications of Contrast-Enhanced Perfusion MRI Techniques in Gliomas: Recent Advances and Current Challenges.* Vol 2017. Contrast Media Mol Imaging; 2017.

33. Ellingson BM, Wen PY, Cloughesy TF. Evidence and context of use for contrast enhancement as a surrogate of disease burden and treatment response in malignant glioma. *Neuro Oncol.* 2018;20(4):457-471.

34. Akbari H, Rathore S, Bakas S, et al. Histopathology-validated machine learning radiographic biomarker for noninvasive discrimination between true progression and pseudo-progression in glioblastoma. *Cancer.* 2020;126(11):2625-2636.

35. Liesche-Starnecker F, Prokop G, Yakushev I, et al. Visualizing cellularity and angiogenesis in newly-diagnosed glioblastoma with diffusion and perfusion MRI and FET-PET imaging. *EJNMMI Res.* 2021;11(1):72.

36. Chen L, Liu M, Bao J, et al. The correlation between apparent diffusion coefficient and tumor cellularity in patients: a meta-analysis. *PLoS One.* 2013;8(11):e79008.

37. Chang PD, Malone HR, Bowden SG, et al. A Multiparametric model for mapping cellularity in glioblastoma using radiographically localized biopsies. *AJNR Am J Neuroradiol.* 2017;38(5):890-898.

38. Yu H, Wen X, Wu P, et al. Can amide proton transfer-weighted imaging differentiate tumor grade and predict Ki-67 proliferation status of meningioma?. *Eur Radiol.* 2019;29(10):5298-5306.

39. Park JE, Kim HS, Park SY, Jung SC, Kim JH, Heo HY. Identification of early response to anti-angiogenic therapy in recurrent glioblastoma: amide proton transfer-weighted and perfusion-weighted MRI compared with diffusion-weighted MRI. *Radiology.* 2020;295(2):397-406.

40. Bulik M, Jancalek R, Vanicek J, Skoch A, Mechl M. Potential of MR spectroscopy for assessment of glioma grading. *Clin Neurol Neurosurg.* 2013;115(2):146-153.

41. Horská A, Barker PB. Imaging of brain tumors: MR spectroscopy and metabolic imaging. *Neuroimaging Clin N Am.* 2010;20(3):293-310.

42. Barajas RF, Jr, Phillips JJ, Parvataneni R, et al. Regional variation in histopathologic features of tumor specimens from treatment-naive glioblastoma correlates with anatomic and physiologic MR Imaging. *Neuro Oncol.* 2012;14(7):942-954.

Acknowledgments

Supplemental digital content is available for this article at neurosurgery-online.com.

Supplemental Digital Content 1. Flowchart for the subjects included in each stage of the tumor probability map (TPM) model development.

COMMENTS

This study represents a significant step forward in the field of neuro-oncology, particularly in the treatment and surgical approach to glioma. By leveraging autopsy tissue samples aligned with clinical MRI, the authors have developed a novel artificial intelligence tool capable of detecting invasive tumor areas beyond traditional imaging boundaries. This approach, which contrasts with previous studies limited to biopsy samples within resectable margins, offers a more comprehensive understanding of tumor presence beyond contrast enhancement and FLAIR hyperintensity.

The methodology, involving a retrospective study design with a substantial sample size and an impressive ensemble algorithm for pixelwise tumor prediction, is rigorously executed. The findings that a

significant proportion of patients had tumor invasion outside the contrast region, with clear links to survival outcomes, underline the importance of this research. Such advancements are crucial for enhancing tumor mapping techniques and potentially extending the treatable margin for gliomas.

While the study's limitations are acknowledged, including the time gap between the last MRI and autopsy samples, these do not significantly detract from the overall validity and impact of the research. The predictive maps generated are a promising tool, offering a pathway for more accurate tumor identification and potentially improving survival outcomes. However, further clarification on the application of these maps, whether for maximizing resection or clinical monitoring, would enhance the study's coherence.

The inclusion of both gliomas and GBMs raises questions about the handling of non–contrast-enhancing aspects in the study. Additionally, the consideration of tumor genetics and other confounding factors in glioma prognosis would provide a more comprehensive understanding of the study's implications.

In summary, this research is a commendable and essential addition to the literature. It not only advances our understanding of glioma mapping and treatment but also sets a precedent for future studies in the field. The potential for these findings to influence clinical practices and improve patient outcomes is substantial, marking a pivotal moment in the journey toward more effective glioma treatment strategies.

David Jaehyun Park, MD, PhD
Palo Alto, California, USA

The authors should be commended for developing tools to identify glioma infiltration probability maps. In glioma surgery, cytoreduction through surgically removing tumor improves survival. Not all tumor regions have similar tumor cell density. For example, the majority of progression of glioblastoma occurs within 2 centimeters of the contrast-enhancing tumor. Recent work by Molinaro et al (2020) demonstrated that supramaximal resection of T2 FLAIR regions improves survival in GBM. Aggressive removal of T2 FLAIR signals in GBM is limited by large volumes of FLAIR signal in some patients and risks for new neurological deficits. Identifying high-risk tumor regions within FLAIR signals can help guide surgical resection, making us more successful surgeons. To accomplish this task, the authors developed an ensemble algorithm which utilizes routine MRI images to generate tumor infiltration probability maps based on cellularity, extracellular fluid, and cytoplasm density. The innovation for this group is developing radio-pathomic models using MRI brains of recently deceased patients with GBM. When applied to a sample set of patients with imaging and autopsy results, the algorithm produced density maps that reliably identified infiltration beyond enhancing areas, and the presence of this spread was associated with poorer survival. This technique requires further validation to demonstrate its accuracy in larger data sets; however, it represents a powerful new tool in evaluation of patients and planning for intervention. One major limitation in the current form is the use of only the MR images collected closest to patient death. Inclusion of longitudinal imaging to track progression would significantly improve the value of the technique.

Ryan A. Cloyd, MD, PhD, Matthew Pease, MD, and Angela M Richardson, MD, PhD
Indianapolis, Indiana, USA